1985

High Dispersion Untraviolet Spectra of the Peculiar Star RX Puppis

Menas Kafatos
Chapman University, kafatos@chapman.edu

A. G. Michalitsianos
NASA, Goddard Space Flight Center

R. P. Fahey
NASA, Goddard Space Flight Center

Recommended Citation
Kafatos, M., Michalitsianos, A.G., Fahey, R.P. (1985) High Dispersion Untraviolet Spectra of the Peculiar Star RX Puppis, *The Astrophysical Journal Supplement Series*, 59: 785-798. doi: 10.1086/191085

High Dispersion Untraviolet Spectra of the Peculiar Star RX Puppis

THE ASTROPHYSICAL JOURNAL SUPPLEMENT SERIES, 59:785–798, 1985 December

HIGH-DISPERSION ULTRAVIOLET SPECTRA OF THE PECULIAR STAR RX PUPPIS

M. KAFATOS[1]
Department of Physics, George Mason University, Fairfax, Virginia
A. G. MICHALITSIANOS[1] AND R. P. FAHEY
Laboratory for Astronomy and Solar Physics, NASA/Goddard Space Flight Center, Greenbelt, Maryland
Received 1985 January 9; accepted 1985 June 19

ABSTRACT

High spectral resolution observations of the peculiar star RX Puppis obtained with the *International Ultraviolet Explorer* suggest the presence of a complex gaseous ring system which surrounds an accreting hot secondary. The anomalous line intensity ratio of the C IV λλ1548, 1550 doublet during the observations exceeded the optically thick limit, implying the presence of a high-velocity wind. Additionally, the C IV doublet exhibits about four or five narrow emission components, which are redshifted up to velocities of at least $\sim +300$ km s^{-1} (with respect to the rest wavelength).

Subject headings: stars: binaries — stars: emission-line — stars: individual — ultraviolet: spectra

I. INTRODUCTION

The peculiar object RX Puppis is characterized by a variety of emission which occurs at radio, infrared, and ultraviolet wavelengths. Its optical spectrum exhibited strong Balmer and nebular emission lines in the early 1940s (Swings and Struve 1941). Recently, this star has been returning to the high-excitation phase (Klutz and Swings 1981) after a quiescent phase lasting nearly 20 years. During this phase RX Pup had the appearance of a Be star. The presence of a Mira variable in the system was suggested from 1–4 μm photometry (Feast, Robertson, and Catchpole 1977), and by the presence of H_2O absorption (Barton, Phillips, and Allen 1979). A 580 day period of intensity variations of the Mira variable was subsequently deduced from IR photometry by Whitelock *et al.* (1983). The presence of both infrared and high-excitation nebular line emission has placed RX Pup in a distinct category of composite emission objects classified as dust-associated (D-type) symbiotic stars.

RX Puppis exhibits variable complex line profile structure at both optical and UV wavelengths. Multicomponent P Cygni profiles were found in the Balmer lines by Klutz, Simonetto, and Swings (1978). Two high-dispersion UV spectra of RX Pup obtained in 1980 with the *International Ultraviolet Explorer* (*IUE*) and reported by Kafatos, Michalitsianos, and Feibelman (1982) indicated electron densities in the line-emitting region of $\sim 10^9$–10^{11} cm^{-3}, and dimensions of $\lesssim$ a few $\times 10^{13}$ cm. The presence of high-excitation permitted and intercombination lines, and strong UV continuum throughout the wavelength range of the *IUE*, was attributed to intense photoionizing radiation from a hot ($T_{\rm eff} \sim 75{,}000$–$90{,}000$ K) subdwarf. The sharp, doubled, and multicomponent structure seen in strong permitted and intercombination emission lines in the short-wavelength range of the *IUE* (SWP, λλ1200–2000) indicated that perhaps streamers or a complex gaseous ring system was present. In this paper we report results of the analysis of all five high-resolution (HIRES) *IUE* spectra of RX Pup which were obtained between 1980 September and 1984 March. Our observations show strong variations in the profiles of the prominent lines which characterize far-UV spectra of RX Pup. The implications which these observations have for several models for high-excitation emission in peculiar emission stars are discussed.

II. OBSERVATIONS

Five high- and low-dispersion *IUE* spectra have been obtained of RX Pup in the SWP λλ1200–2000 and LWR λλ2000–3200 cameras using the large (10″ × 20″) entrance aperture; *IUE* instrumentation is described by Boggess *et al.* (1978). In Table 1 the exposure times and image sequence numbers for particular observing epochs are shown. In Table 2 absolute emission-line fluxes from low-dispersion spectra (~6 Å resolution) are given for prominent emission lines; these values are not corrected for interstellar extinction. Over the 4 year course of observations, emission-line fluxes generally exhibited brightening which reached maximum between 1981 June 11 and 1983 March 22 and was followed by a gradual decline in intensity over ~1 year. The total absolute flux variations in the C IV λλ1548, 1550 doublet were ~30%, while the He II λλ1640, 2511, 2733 lines exhibited larger variations, ranging up to ~70% in λ2511. Similarly, Mg II λλ2795, 2802 showed extremes of ~80% from maximum to minimum UV light. Most of the intercombination lines such as C III] λλ1907, 1909, O IV] λλ1400–1407, N IV] λ1487, O III] λλ1660, 1666, and N III] λλ1749–1754 exhibited enhancements of about ~20%, which was followed by a general decline in flux from maximum on 1984 June 11 to March 11. In Figures 1*a*–1*d*, the strongest emission lines in the SWP wavelength range of the *IUE* for all five epochs are shown.

A few lines exhibited distinctly different behavior. For example, Si III] λ1892 continually declined in absolute inten-

[1]Guest Observer, *International Ultraviolet Explorer*.

sity between 1980 September 20 (first observations) and 1984 March 11 (last observations), in contrast to the temporal behavior of most of the other intercombination and permitted lines during this same period. The appearance of the high-excitation N V λλ1239, 1243 doublet on 1983 October 29 and 1984 March 11 during the declining emission phase is unexpected and not easily explained, unless a drop in the extinction inherent in the system allows high-excitation radiation to escape from the inner regions near the hot star.

Of particular interest in high-dispersion *IUE* spectra is the complex nature of the strong intercombination and permitted line profiles. In our initial high-resolution *IUE* observations (1980 September 20) of RX Pup (Kafatos, Michalitsianos, and Feibelman 1982), we found that He II, N III], N IV], O III], and Si III] exhibited double-peak structure. The C IV λλ1548, 1550 doublet profiles are significantly more complex (Fig. 1*b*), showing multiple discrete emission components that are displaced redward of the laboratory rest wavelength (λ_0), and which combine to extend the red wings. We note that extended red wing emission in C IV has been reported for a similar object, HM Sge, by Mueller and Nussbaumer (1985). Redward-displaced emission components appear to be a constant feature of the C IV doublet structure over the 4 year course of *IUE* observations, with only several weak blueward peaks with velocities ranging up to -100 km s^{-1} appearing in some observations. Both the redward displaced components and the total absolute flux changed in relative intensity with respect to one another between the first and last observations (1980 September 20 and 1984 March 11). However, the C IV line emission component remained consistently redward with respect to the rest wavelength for all five observing epochs.

Because the widths of the sharp emission components seen in the C IV λλ1548, 1550 profiles are comparable to the resolving limit of HIRES SWP spectra, caution must be taken to ensure that these features are real, and are not an artifact of detector noise or the extraction process. The broadened C IV HIRES profiles are quite evident from the *IUE* photowrites. Generally, the strong emission lines are well exposed in 240–300 minutes, with C IV typically achieving ~150 DN, with a background noise level of 40–50 DN, i.e., expected for these exposure times. For each sharp emission component suspected of being real in the C IV λ1548 profile, its counterpart at λ1550 had to be identified at +2.6 Å, in order to establish this velocity feature as real. Five to six discrete components were so identified. In Table 3 the velocities shown (with respect to the laboratory rest wavelength λ_0) are averages of the individual velocities associated with a given C IV

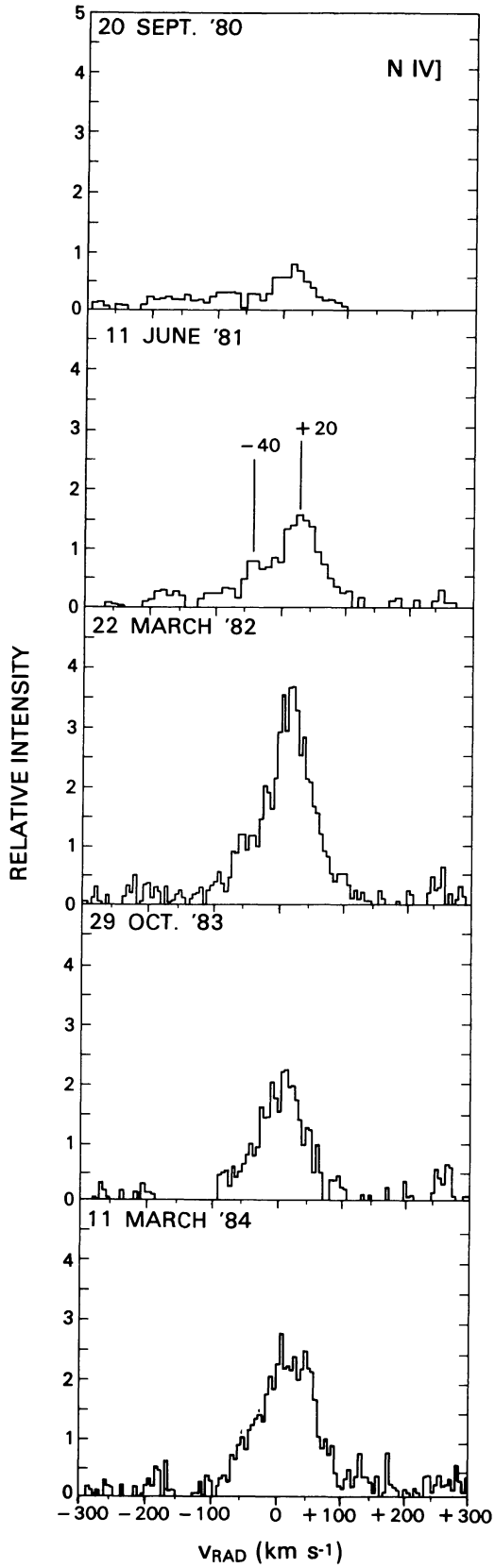

FIG. 1*a*

FIG. 1.—High-resolution line profiles observed for five *IUE* observing epochs in the SWP wavelength range of the *IUE* are shown in velocity space. Note that the radial velocity at 0 km s^{-1} corresponds to the laboratory rest wavelength and is not corrected for radial velocity. Smoothing or pixel averaging has not been applied to these profiles. Line emission is expressed in relative intensity for a given epoch exposure, and as such is not in absolute units. Hence, a quantitative comparison of line intensities for different epochs yields only qualitative indications for flux variations. Temporal variations in the absolute line fluxes for UV emission lines is obtained from low-resolution *IUE* SWP and LWR/LWP exposures. (*a*) N IV] λ1486.5 intercombination line reached maximum intensity on 1982 March 22. The line profile is extended mostly in the blue wing, with sharp emission components appearing at all epochs.

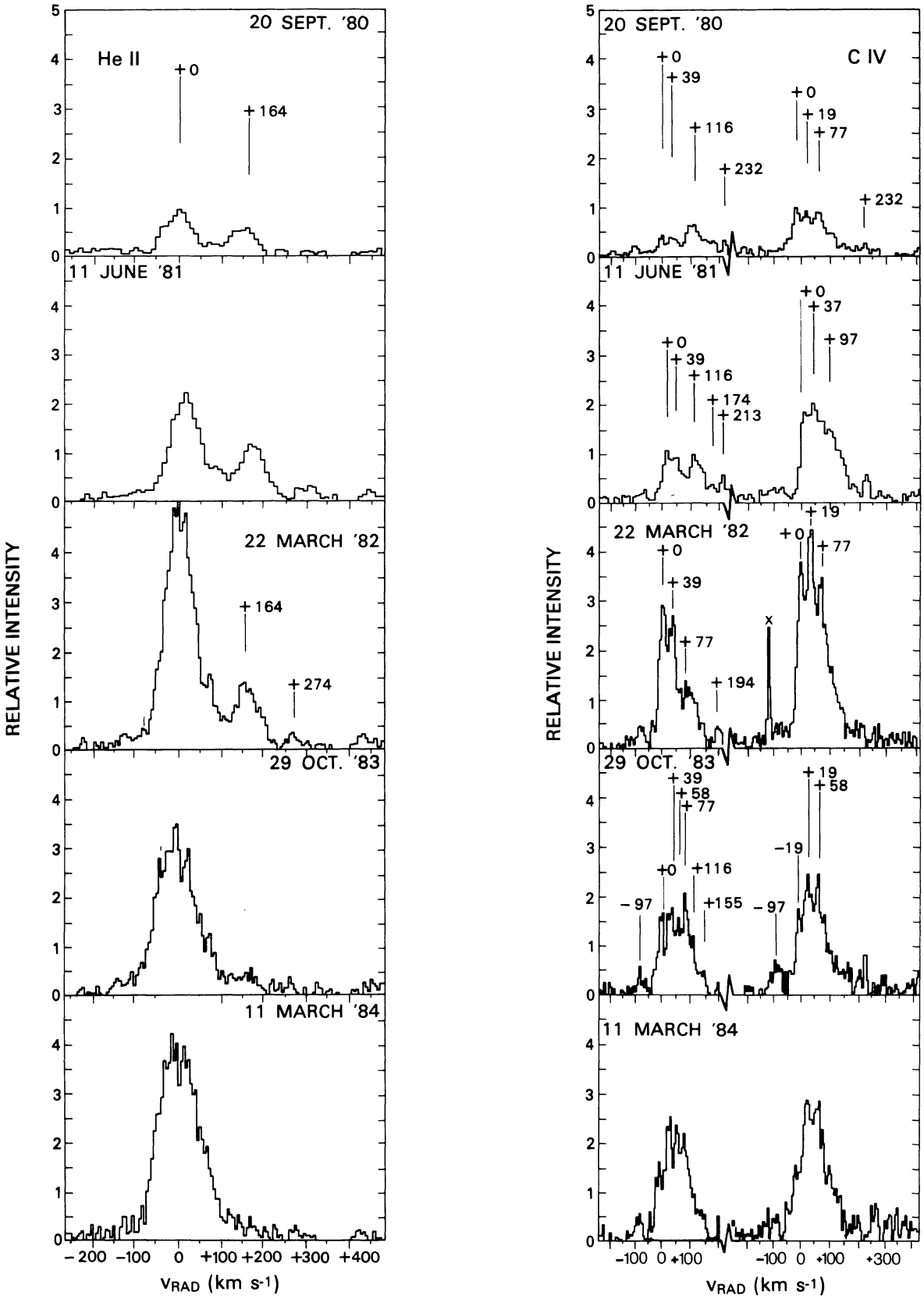

FIG. 1*b*.—(*Left*) He II λ1640.3 exhibited two broad emission peaks. Primary emission enhancement on 1982 March 22 occurred at the laboratory rest wavelength, with the redward-displaced component at $\sim +164$ km s^{-1} showing only modest enhancements at this epoch. The appearance of extended wings and broadened structure in the far red wings of the line are noted. (*Right*) C IV λλ1548.2, 1550.7 exhibit up to seven distinct sharp emission components on 1982 March 22, where the doublet intensities exceed the optically thick limit at this epoch in particular. Exposures were never sufficiently long to discern the adjacent continuum. Cross indicates detector particle noise.

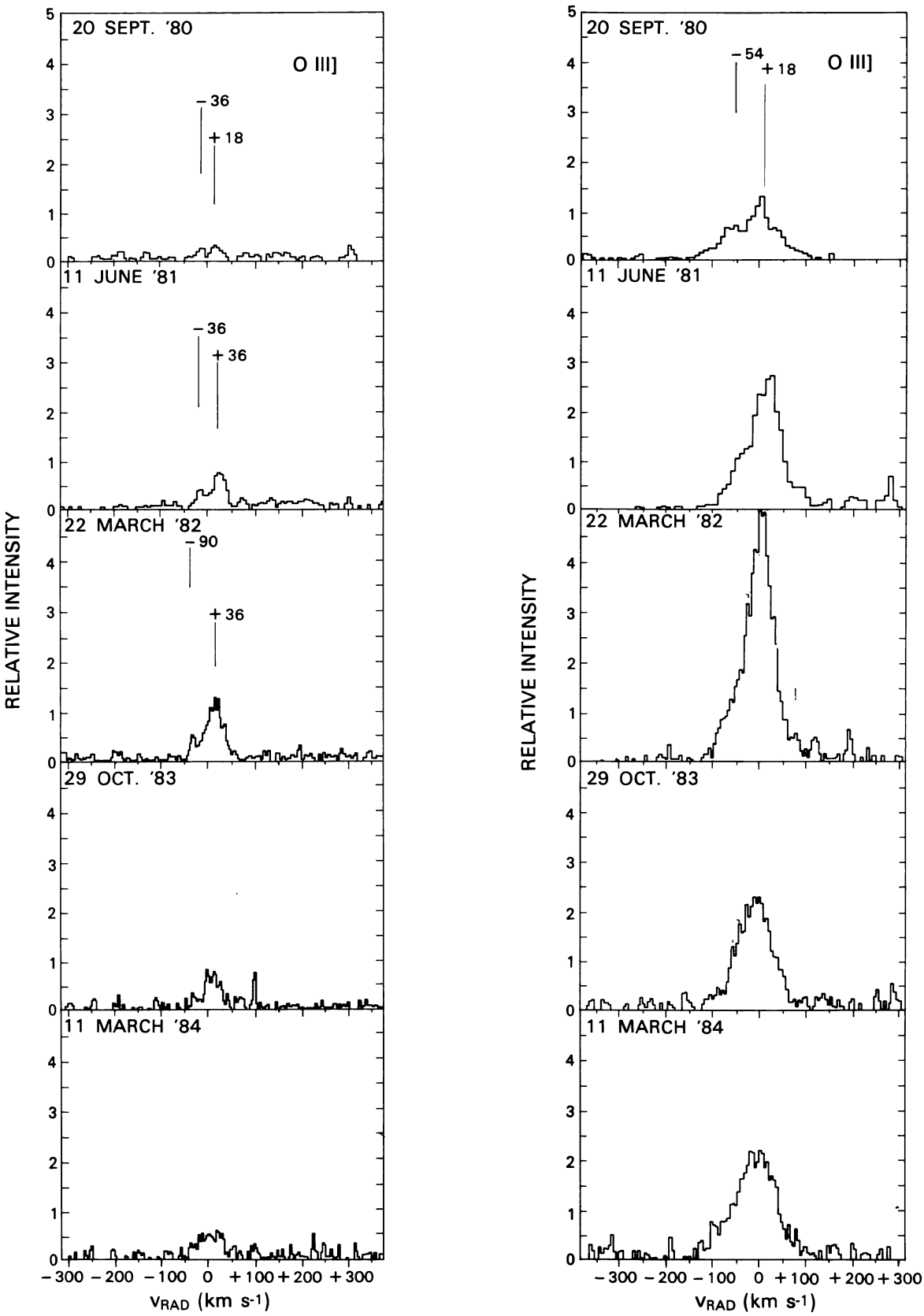

FIG. 1c.—O III] λλ1666.8, 1666.2 intercombination lines exhibited doubled intensity profiles, nearly symmetrically placed about the rest wavelength. At maximum UV light on 1982 March 22 the blueward component of the 1666.2 Å line is unresolved, giving the appearance of an extended blue wing.

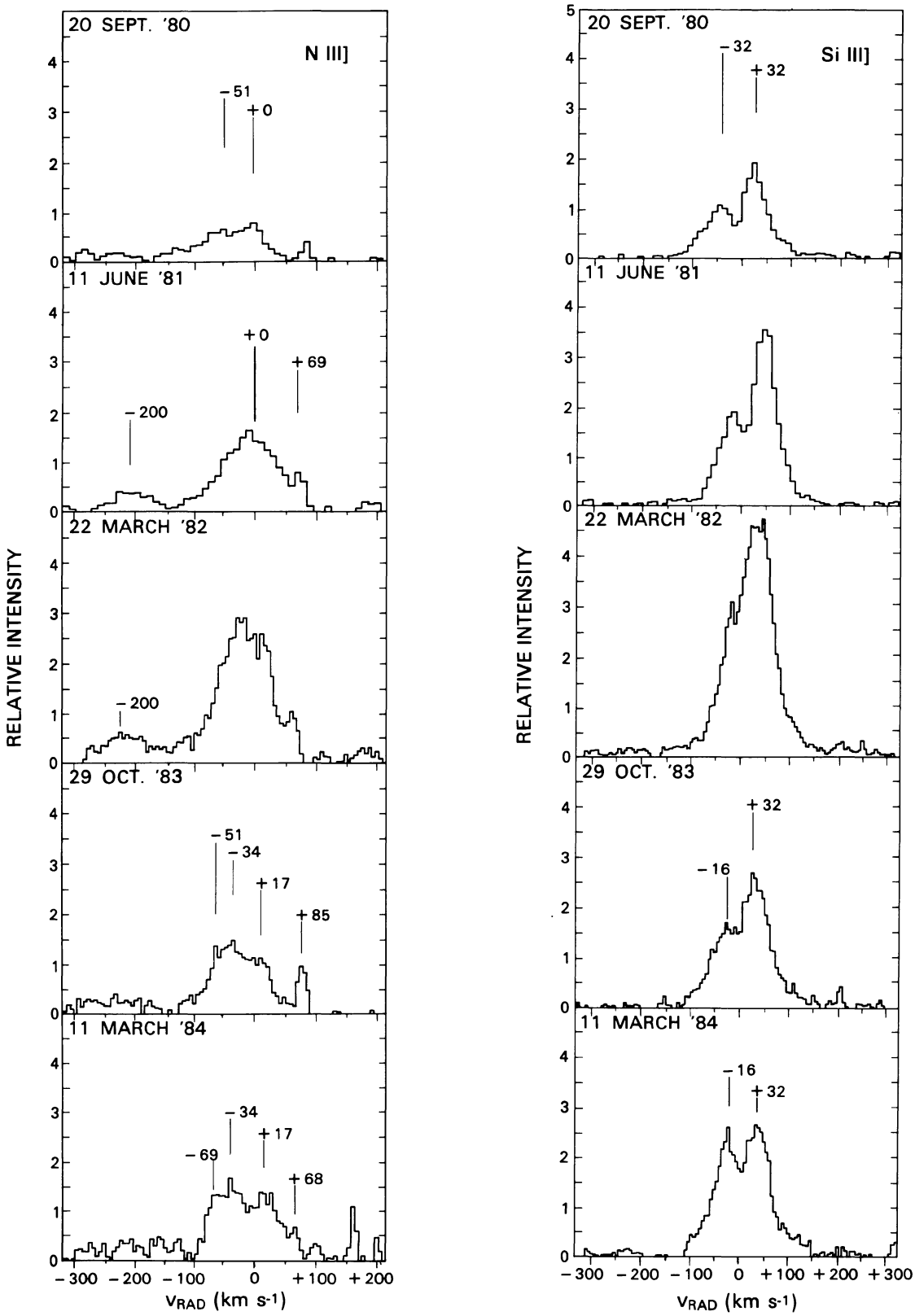

FIG. 1*d*.—(*Left*) N III] λλ1748.6, 1749.7, 1752.2, 1754.0 intercombination multiplet exhibits complex structure at all epochs, with a second strong emission component appearing during maximum on 1982 March 22 at −200 km s^{-1}. Because N III] consists of four strong multiplets, confusion results if we attempt to assign particular features to each of the multiplets in velocity space. Accordingly, the velocity scale is shown with respect to λ1749.7 at 0 km s^{-1}, the component generally strongest in optically thin emitting regions. (*Right*) Si III] λ1892.0 intercombination line exhibits two clearly resolved components at all epochs. The line-profile structure on 1982 March 22 indicates that emission at the rest wavelength increased substantially as the wings broadened. The secondary component visible in the blue wing of the stronger emission line is just resolvable at maximum light, but both components are roughly of equal intensity on 1984 March 11, when the system has nearly recovered to its initial state. Note that C III] λλ1906.8, 1908.7 (not shown here) was generally saturated during these exposures. A suggestion for double structure is indicated in several spectra, but observing allocated time did not permit additional shorter exposed spectra to determine C III] line-profile structure. We suspect, however, double structure in C III] as is evident in Si III], which never achieved saturation.

TABLE 1

IUE OBSERVATION PROGRAM

DATE	CAMERA SWP	CAMERA LWR/LWP	EXPOSURE (min)	HIGH (H)/LOW (L) RESOLUTION
1980 Sep 20	10189	...	45	L
	10190	...	15	L
	...	LWR 8856	30	L
	10191	...	102	H
1981 Jun 11	...	LWR 10830	20	L
	14239	...	15	L
	14240	...	180	H
	...	LWR 10831	120	H
	...	LWR 10832	8	L
1982 Mar 22 ...	...	LWR 12837	80	H
	16598	...	15	L
	...	LWR 12838	20	L
	16597	...	300	H
1983 Oct 29 ...	21402	...	240	H
	...	LWP[a] 2177	85	H
	21403	...	15	L
	...	LWP 2176	15	L
1984 Mar 11 ...	...	LWP 2924	15	L
	22461	...	285	H
	22462	...	15	L

[a]LWP replaced LWR camera.

TABLE 2

TEMPORAL VARIATIONS IN STRONG UV EMISSION LINES IN RX PUPPIS

ION	λ (Å) (LABORATORY)	1980 Sep 20 λ (Å) *IUE*	1980 Sep 20 Flux[a]	1981 June 11 λ (Å) *IUE*	1981 June 11 Flux[a]	1982 Mar 22 λ (Å) *IUE*	1982 Mar 22 Flux[a]	1983 Oct 29 λ (Å) *IUE*	1983 Oct 29 Flux[a]	1984 Mar 11 λ (Å) *IUE*	1984 Mar 11 Flux[a]
N V	1238.8, 1242.8	...	...	...	...	...	...	1240.8	0.5	1240.2	0.7
O I	1304.5, 1306.0	1303.4	0.7	1303.6	0.6	1304.2	1.2	...	...	1304.4	0.1
Si IV	1393.7	1392.6	0.4	1394.2	0.3	1394.0	0.4	1394.4	0.4	1393.0	0.1
O IV]	1399.8, 1401.1 / 1404.8, 1407.4	1401.6	0.7	1403.2	0.9	1403.8	1.5	1403.2	1.4	1405.0	1.4
N IV]	1486.5	1484.6	2.3	1486.2	3.4	1486.8	3.2	1487.4	2.7	1485.8	3.0
C IV	1548.2, 1550.7	1549.0	10.0	1550.4	11.4	1550.8	11.0	1551.8	8.8	1550.6	8.3
He II	1640.3	1639.2	3.6	1640.0	5.0	1641.2	5.4	1641.8	5.6	1650.6	5.3
O III]	1660.8, 1666.2	1664.4	5.4	1666.2	5.6	1666.6	4.8	1668.0	3.4	1665.4	3.2
N III]	1748.6, 1749.7 / 1752.2, 1754.0	1749.0	3.2	1750.6	3.5	1751.4	3.4	1752.2	2.2	1751.0	2.0
[Ne III]	1814.8	1815.6	weak	1817.4	weak	...	...	...	...	...	...
Si III]	1892.0	1889.6	3.5	1892.0	3.1	1892.8	3.0	1894.0	2.1	1892.2	1.8
C III]	1906.8, 1908.7	1906.8	7.7	1908.0	9.1	1909.2	9.5	1910.4	7.7	1908.4	7.8
He II	2511.2	2510.8	0.4	2511.8	1.0	2509.0	0.9	2509.6	0.3	2510.8	0.3
He II	2733.2	2734.6	0.8	2737.0	0.6	2737.4	0.7	2735.4	0.4	2736.2	0.3
Mg II	2795.5, 2802.7	2800.2	2.2	2796.6	10.1	2799.6	4.9	2799.0	2.8	2800.2	2.8
He I + [Ar IV]	2829.1, 2853.6	2842.4	2.6	2838.0	3.4	2837.6	4.7	2837.4	2.1	2831.0	2.1
He I + O III	3013.7, 3024.6	3024.8	0.1	...	...	3023.4	0.7	3024.8	0.4	3025.4	0.3
O III	3047.1	3046.8	1.0	3049.8	0.9	3048.2	1.6	3048.6	0.9	3048.8	0.9
O III	3132.9	3133.6	5.2	3136.0	8.8	3132.4	10.4	3140.0	6.7	3134.4	6.4

[a]Flux in units of 10^{-12} ergs cm^{-2} s^{-1} (not corrected for extinction). Absolute emission-line fluxes from low-dispersion spectra.

TABLE 3

C IV ABSOLUTE VELOCITY OF SHARP EMISSION COMPONENTS

	VELOCITY (km s^{-1})[a]				
EXPOSURE	*a* (1980 Sep 20)	*b* (1981 Jun 11)	*c* (1982 Mar 22)	*d* (1983 Oct 29)	*e* (1984 Mar 11)
1	+ 9	−61	−77	−89	−75
2	+39	+17	−33	−11	− 5
3	+97	+45	+ 5	+23	+34
4	+233	+109	+35	+54	+64
5	+309	+186	+85	+78	+86
6	...	+232	+212	+233	+118

[a]With respect to laboratory rest wavelengths for C IV λλ1548.2, 1550.7. Velocities shown are averages for components identified in lines λλ1548 and 1550.

NOTE.—Uncertainties in absolute wavelength calibration in the SWP camera are $\Delta\lambda \sim 0.05$–0.1 Å (10–20 km s^{-1}).

emission pair. We were unable to correct for radial velocity because an estimate from optical spectroscopy does not presently exist. We believe, however, that RX Pup has a very modest radial velocity of not greater than ± 10 km s^{-1}. This follows because the star lies close to the Galactic plane, i.e., $l = 258°$, $b = -4°$. From Table 3 it is evident that most of the emission components lie redward of λ_0, with extremes in velocity generally ranging up to $\lesssim +233$ km s^{-1}, and in one epoch (1980 September 20) as high as $+309$ km s^{-1}.

Our longest exposures of 300 minutes in the SWP camera, however, were not sufficient to discern continuum emission as far as ± 1000 km s^{-1} with respect to λ_0. Accordingly, the absorption components associated with broad P Cygni–type structure are not directly evident in our data. Rather, only the broad emission component of the P Cygni profile is seen. However, the relative line intensities of the C IV doublet provide a strong indication for the presence of a broad P Cygni absorption trough, that extends to velocities of at least $\gtrsim -800$ km s^{-1}. In Figure 2 we have plotted the intensity ratio of the C IV doublet against the total absolute C IV emission flux for all five observing epochs (normalized to absolute emission on 1980 September 20). The tendency is apparent for the doublet ratio to decline with increasing C IV flux, implying that the ratio becomes less than the value of the optically thick limit $I(\lambda 1548)/I(\lambda 1550) = 1$. We are not aware of any other mechanism besides absorption of the 1548 Å line that can reduce the doublet ratio in this fashion, as has also been noted for AG Pegasi (cf. Keyes and Plavec 1980). It is of further interest to note that unusual C IV doublet intensities have also been reported for the D-type symbiotic HM Sge (Mueller and Nussbaumer 1985). The C IV $I(\lambda 1548)/I(\lambda 1550)$ ratio had an observed value ~ 1.1 prior to a sudden increase in high-excitation line emission in C IV, He II, N IV], and N V. Following the ~ 1 month period of line emission brightening in HM Sge, the C IV doublet had an observed value ~ 1.5, i.e., closer to the expected theoretical value of $I(\lambda 1548)/I(\lambda 1550) = 2$, for optically thin emission. RX Pup appears to exhibit much greater absorption at 1548 Å than HM Sge, where the C IV ratio never exceeded unity during the course of our *IUE* observations. However, following a period of enhanced emission in high-excitation lines, the C IV ratio in RX Pup did increase in much the same manner as reported for HM Sge.

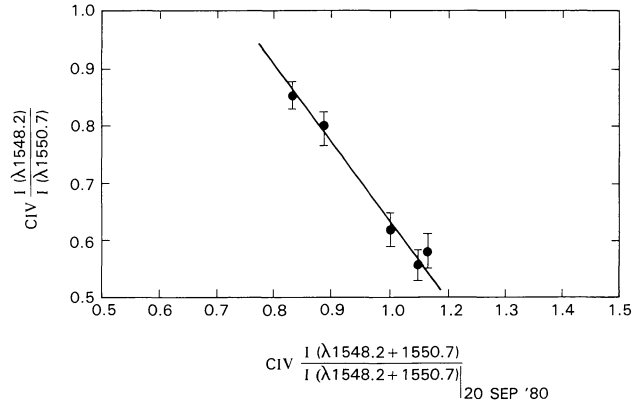

FIG. 2.—C IV doublet intensity ratio $I(\lambda 1548.2)/I(\lambda 1550.7)$ plotted against the combined doublet absolute line flux $I(\lambda 1548.2 + \lambda 1550.7)$, normalized to the combined C IV absolute line intensities of 1980 September 20. Note that the doublet ratio is generally $\lesssim 1$, and the optically thick limit is always exceeded, especially as the combined line flux intensity increases. This is consistent with enhanced material in a wind during outbursts, in which 1550.7 Å P Cygni line-profile absorption affects emission at 1548.2 Å; this corresponds to a minimum wind velocity of $\gtrsim 500$ km s^{-1}, i.e., C IV doublet separation $\Delta\lambda = 2.59$ Å.

If the anomalous C IV doublet intensities are the result of strong absorption of the 1548 Å component by the broad 1550 Å P Cygni line, this behavior suggests that enhanced UV line emission in RX Pup coincides with mass expulsion (probably in the form of a stellar wind). Accordingly, we deduce a minimum wind velocity of at least 700–800 km s^{-1}, obtained from a wavelength separation in the C IV doublet lines ($\Delta\lambda = 2.6$ Å) of approximately 500 km s^{-1}, and an additional 200–300 km s^{-1} for the most redshifted components. We conclude that the broad P Cygni absorption component associated with the 1550 Å line would weaken the emission strength of the 1548 Å component, especially during outbursts.

Moderate wind velocities (~ 60 km s^{-1}) are seen in the Mg II λλ2795, 2802 profile observed on 1982 March 22. Since Mg II emission generally reflects lower excitation conditions with characteristic nebular temperatures ($\sim 10^4$ K), the lower velocities indicated in Mg II suggest that a deceleration in the

wind occurs in the more extended cooler regions, which we estimate to be 10 times greater in extent than the more compact high-excitation C IV emitting region, the latter being $\sim 10^{13}$ cm (see § IV).

Substantial changes in both line-profile structure and emission intensity in the C IV λλ1548, 1550 doublet are indicated in Figure 3*a*. We also show high-resolution He II, O III], and Si III] spectra for all five epochs (Figs. 3*b*–3*d*). The profiles were smoothed using a 3-point running average in order to remove high-frequency noise. Any feature which survives the filter is more likely to be part of the stellar spectrum than an artifact of the sampling technique or data reduction. We estimate a limiting spectral resolution in the SWP spectra of $\Delta\lambda \sim 0.1$ Å at 1550 Å, which corresponds to ~ 20 km s^{-1}. Sharp emission components (evident in the *IUE* photowrite images) redward of the rest wavelength characterize the profile of structure of the 1550.7 Å component (especially at maximum emission) after averaging. Multiple-component structure is seen in other atomic species, such as He II, O III], and Si III] even after smoothing has been applied (Figs. 3*b*–3*d*). Vertical marks shown for the C IV λ1550 line (Fig. 3*a*) indicate the velocity position of sharp emission components in line profile c that are separated by a constant velocity interval $\Delta V \sim 30$–40 km s^{-1}. These sharp components appear to repeat three or possibly four times, and are most apparent when the line emission is a maximum. Profiles d and e exhibit similar sharp emission structures which coincide in velocity space with those of profile c. Note that the relative velocity differences $\Delta V \sim 30$–40 km s^{-1} are not readily apparent from the absolute velocities shown in Table 3. We attribute this to uncertainties in the *IUE* absolute wavelength calibration that introduce errors of the order of $\sim \pm 15$ km s^{-1} (0.05–0.1 Å). It should be noted that all of these observations, with the exception of the first, were corrected for spacecraft motion, and the correction is at most ± 4 km s^{-1}.

Although the intensities of the sharp redward components have changed relative to one another at each epoch, the position of the peaks in velocity space appears stationary over 4 years, to within the accuracy of the high-dispersion SWP wavelength calibration, ± 0.1 Å. Note that the entire profile for 1981 June 11 (b) appears systematically redshifted by $\sim +20$ km s^{-1} with respect to the other four epochs. Because this shift is evident in C IV, He II, and the intercombination lines, it probably represents a wavelength calibration error in this particular epoch that is present in all echelle orders.

III. DATA ANALYSIS

The high-resolution C IV and He II profiles of RX Pup are very similar to each other over the five epochs. We identify four or five redshifted components that range in velocity from $\sim +5$ km s^{-1} to $\sim +300$ km s^{-1}. Several blueshifted components appear which have velocities of ~ -100 km s^{-1}. The semiforbidden profiles show considerably simpler profile structure. They are more symmetric around zero velocity, the peaks corresponding to $\sim \pm 30$ km s^{-1}. The redshifted component tends to be stronger, although at epoch d several peaks have comparable intensity. Doubled line-profile structure is also evident in He II (epochs d and e) and even in C IV (profile c). Weak components at $\sim \pm 150$ km s^{-1} are evident in the O III] and Si III] lines at epoch c.

We have considered a number of geometries and models to explain these complicated profiles. Of these we have excluded the following:

1. *Accelerated-collimated mass flow.*—If the discrete line-forming regions were undergoing acceleration, we certainly would not expect the components to remain stationary in velocity space over 4 years. For example, a parcel of gas moving at even a moderate speed of ~ 100 km s^{-1} will move $\sim 10^{15}$ cm, or ~ 30 Mira radii, over 4 years. This parcel eventually will collide or merge with slower moving parcels which have attained terminal velocity. Accordingly, these parcels would merge and lose their identity in velocity space at some characteristic speed, probably near the terminal velocity of the system. This is not supported by the behavior of the C IV doublet components. The components identified in our first observations appear to retain their velocity over the 4 year period of observations, only changing in relative intensity. Accelerated motion would result in a systematic shift in velocity space of each identifiable emission component over the course of these observations. Rather, the components appear to remain stationary (indicated by vertical marks in Fig. 3*a*) in velocity space to within the resolution uncertainties of HIRES-SWP spectra ± 0.1 Å (for narrow emission lines).

2. *A simple streamer of gas.*—Unless the orbital period of the system was much greater than 50 years, a streamer would introduce strong geometrical effects over the course of 4 years as the aspect of the system changes.

3. *Colliding winds.*—The characteristic double profiles which are a property of this model—but also of any nonspherical model composed of rings, shells, jets, etc.—are seen here in the semiforbidden lines. However, this model does not account for the complex line-profile structure evident in permitted lines of He II and C IV.

We believe that the only model which can successfully account for all the line-profile properties of RX Pup is a system of rings that surround the hot secondary component (with $M_2 \sim 1\ M_\odot$) and which are embedded in an expanding hot stellar wind. The following arguments support this model:

1. The C IV doublet intensities have a ratio which is inverted in the sense that the 1548 Å line is weaker than the 1550 Å line. The simplest way to interpret this inversion is to assume that a fast wind surrounding both the hot star and the system of rings absorbs some of the emission at 1548 Å with the blueshifted 1550 Å P Cygni absorption trough. A fast wind has already been established from the optical observations of RX Pup by Klutz, Simonetto, and Swings (1978) in the hydrogen Hγ and Hδ lines. Our exposures, however, were not sufficiently long to discern the continuum in the SWP spectra of RX Pup, and therefore could not detect the absorption trough of the C IV profiles. Our redshifted emission components of C IV and He II appear similar to the redshifted components of the hydrogen lines seen by Klutz, Simonetto, and Swings (1978). We note that a 900 km s^{-1} wind is favored for the symbiotic star AG Peg by Penston and Allen (1985), and perhaps a 1700 km s^{-1} wind in HM Sge by Wallerstein (1978).

2. The semiforbidden lines generally show symmetry around 0 km s^{-1} with the two peaks of the doubled profiles $\sim \pm 30$ km s^{-1}. Even though the redshifted component is generally stronger, the two become comparable to each other at epoch

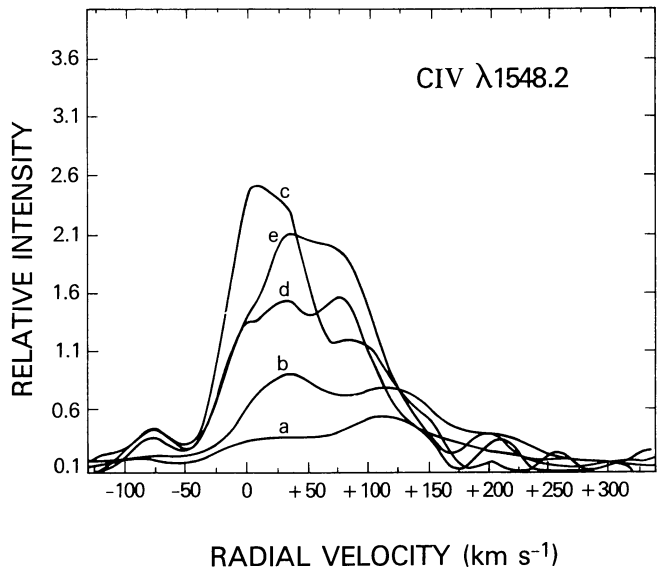

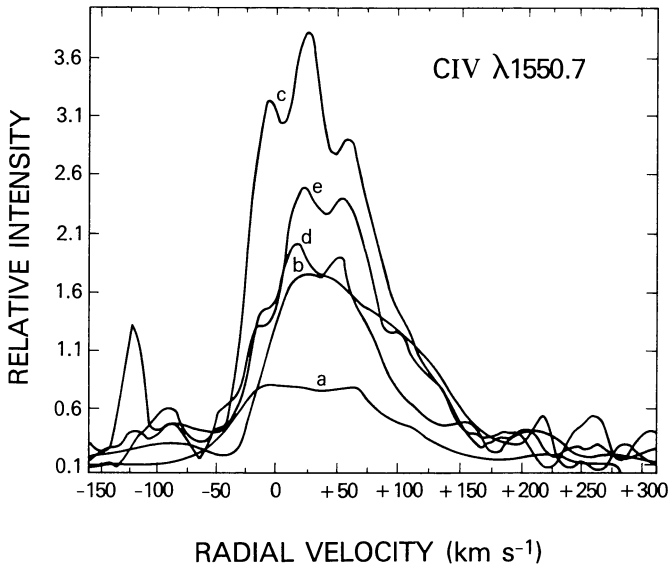

FIG. 3*a*

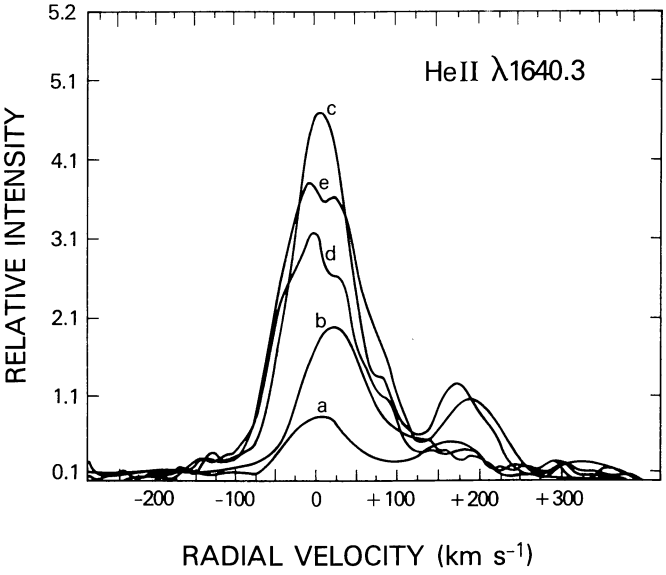

FIG. 3*b*

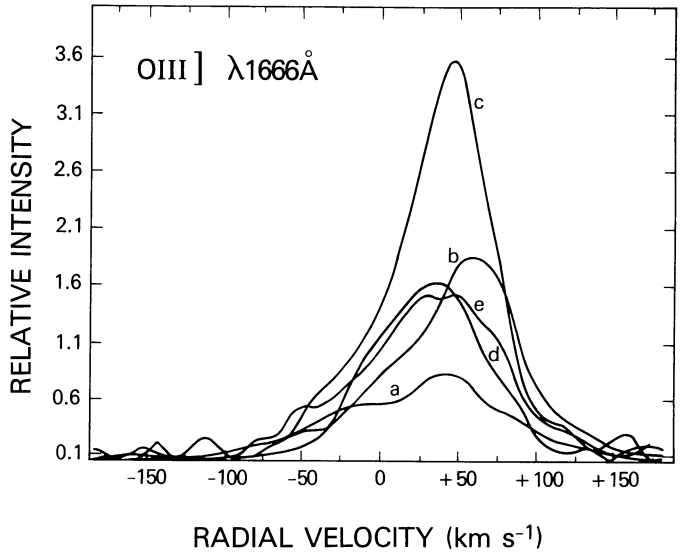

FIG. 3*c*

FIG. 3.—Three-point running average applied to C IV, He II, O III], and Si III] line profiles. Line profiles from each epoch are overplotted in velocity space: epoch a, 1980 September 20; epoch b, 1981 June 11; epoch c, 1982 March 22; epoch d, 1983 October 29; and epoch e, 1984 March 11. (*a*) C IV doublet line profiles. Vertical marks shown on λ1550.7 indicate emission peaks which appear stationary in velocity space for epochs c, d, and e, although their relative intensities with respect to one another have changed. Emission peaks in line profiles a and b are not evident after smoothing, since the total line intensity for these epochs was smaller. (*b*) He II λ1640.3 exhibits multiple structure with a secondary component evident at $\sim +200$ km s^{-1}. Note that epoch b profile is redshifted by $+20$ km s^{-1}, which is also evident in C IV; this shift is attributed to a wavelength calibration error which is seen in all echelle orders. (*c*) O III] λ1666.2 intercombination line exhibited emission mainly redward of the rest wavelength for velocities up to $+50$ km s^{-1}. (*d*) Si III] λ1892 exhibited nearly equal doubled structure nearly symmetric around the rest wavelength. Main brightening in the line occurred at 25–30 km s^{-1}, with the smaller blueshifted peak blending in the wing of the stronger redward component.

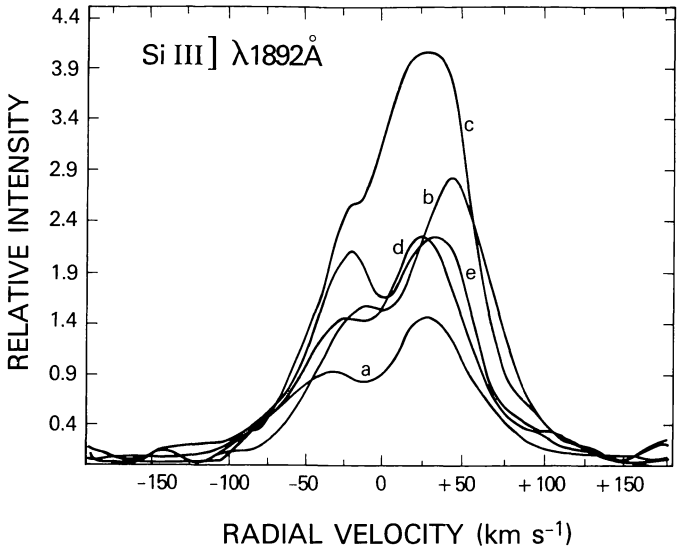

FIG. 3*d*

d, as would be expected for a single ring. We attribute the relative change of the intensity of the two components to viewing the rings from different angles along the orbit of the component stars. As time progresses, one would expect the blueshifted component to become stronger. Similarly, a decline of the red component in C III] λ1909 was seen in HM Sge by Mueller and Nussbaumer (1985) following UV brightening. We also note that the velocity separations they find in semiforbidden lines for HM Sge are comparable to those we find in RX Pup, i.e., 40–50 km s^{-1}.

3. The variation of the $I(\lambda 1548)/I(\lambda 1550)$ intensity ratio over five epochs, in which the optically thick limit is exceeded during enhanced phases of line emission, can be explained in terms of a fast wind becoming more prominent during UV brightening. This point is discussed in § IV. The ratio returns to values of approximately 1:1 as the star returns to quiescence. Even at epochs d and e, however, the wind has weakened and is still present.

IV. DISCUSSION AND CONCLUSIONS

We have seen in § II that the C IV line profiles indicate the presence of at least four redshifted emission components, as well as a couple of blueshifted components. We have investigated the colliding-wind model of Kwok (1982), Wallerstein *et al.* (1984), and Willson *et al.* (1984), which has been developed to explain the optical emission-line profile structure of the peculiar stars V1016 Cyg and HM Sge. Both HM Sge and V1016 Cyg are D-type symbiotics (Allen 1980) that are believed to contain Mira variables as primaries and, therefore, are similar to RX Pup. We can begin by assuming that ~ 20 years is representative of the orbital period of these symbiotics (Willson *et al.* 1984). In the colliding-wind model, we find that the position of the shock region, formed by the collision of the slow wind from the Mira and the high-velocity wind from the hot star, is located near the hot companion, i.e., at $\sim 10^{13}$ cm, with a thickness of the colliding region $\sim 3\times 10^{12}$ cm, if $\dot{M}_{\rm hot\ star} \lesssim 0.1\dot{M}_{\rm Mira}$. On the other hand, if $\dot{M}_{\rm hot\ star} \gtrsim 0.1\dot{M}_{\rm Mira}$, the colliding-wind interface would be at a distance r from the Mira of $r \sim 5\times 10^{13}$ cm, or ~1 Mira radius. Thus, the notion of colliding winds for this particular case is inconsequential. Furthermore, if the interface is located near the Mira, the high velocities suggested from optical and UV spectroscopy are not typical of terminal speeds generally associated with Mira variables.

The density of the Mira wind near the impact region (for head-on collision) is $\sim 10^8$ $(\dot{M}/10^{-6}\ M_\odot\ {\rm yr}^{-1})$ cm^{-3}, and the density of the hot-star wind is $\sim 4\times 10^4(\dot{M}/10^{-10}\ M_\odot\ {\rm yr}^{-1})$ cm^{-3}. It is not clear to us how one could obtain semiforbidden line emission anywhere near the shock region. This emission requires densities of $\sim 10^9$–10^{11} cm^{-3} (Kafatos, Michalitsianos, and Feibelman 1982), which far exceed these expected even for a Mira wind.

Finally, if the mass loss from the Mira is variable (as the luminosity certainly is) over a period of 1–2 years, we would expect periodic changes in the observed line profiles over this time scale. At least for RX Pup, which has a Mira period of 580 days (Whitelock *et al.* 1983), no such periodic changes were observed over a 4 year interval.

As an alternative interpretation, we suggest a model in which rings orbit the secondary. As discussed in §§ II and III, these rings should be embedded in a fast wind that moves away from the secondary. The possibility remains that at least during outburst, the Mira fills its Roche limit. If the binary period is ~ 20 years and the Mira radius is ~ 50% of its Roche radius, moderate eccentricities ($e \sim 0.5$) would allow the Mira to fill its Roche limit near periastron (cf. Kafatos and Michalitsianos 1982).

We have been assuming a Keplerian law of rotation for the system of rings in RX Pup. Therefore, the velocity of a particular C IV emission component determines the radius of the ring. The observed velocities are assumed to be orbital velocities, except for small differences of ~ 20%, which are due to the velocity structure of the ring and its width (Smak 1969; Huang 1972). Moreover, the distances r that we obtain are upper limits. Each distinct emission component has a full width at half-maximum $\Delta w \sim 15$ km s^{-1}, with no systematic change of Δw with increasing radial velocity v. Moreover, component spacing is roughly constant and of the order of $\Delta v \sim 30$ km s^{-1}. This suggests that the rings become wider with increasing radius r; smaller velocities v correspond to larger radii. As can be seen from Table 3, for the observations of 1982 March 22, the three redshifted components at $v \sim +35$, 85, and 212 km s^{-1} correspond to a radial distance $r \sim 1.1\times 10^{13}$, 1.8×10^{12}, and 3×10^{11} cm, respectively. The blueshifted components at $v \sim -33$ and -77 km s^{-1} correspond to $r \sim 1.2\times 10^{13}$ and 2.2×10^{12} cm, respectively. These values assume $\sim 1\ M_\odot$ for the hot companion. The corresponding width of the three rings is estimated at $\Delta r/r \sim 1$, 0.4, and 0.15, respectively. In Figure 4 we show the system of three rings in the plane of the orbit (probably the ring plane). The portion labeled "redshifted" shows the structure of the rings deduced from the redshifted components. The difference in radii of rings deduced from the red- and blueshifted C IV emission components (Fig. 4) reflects uncertainties in the wavelength calibration of high-resolution SWP spectra. The

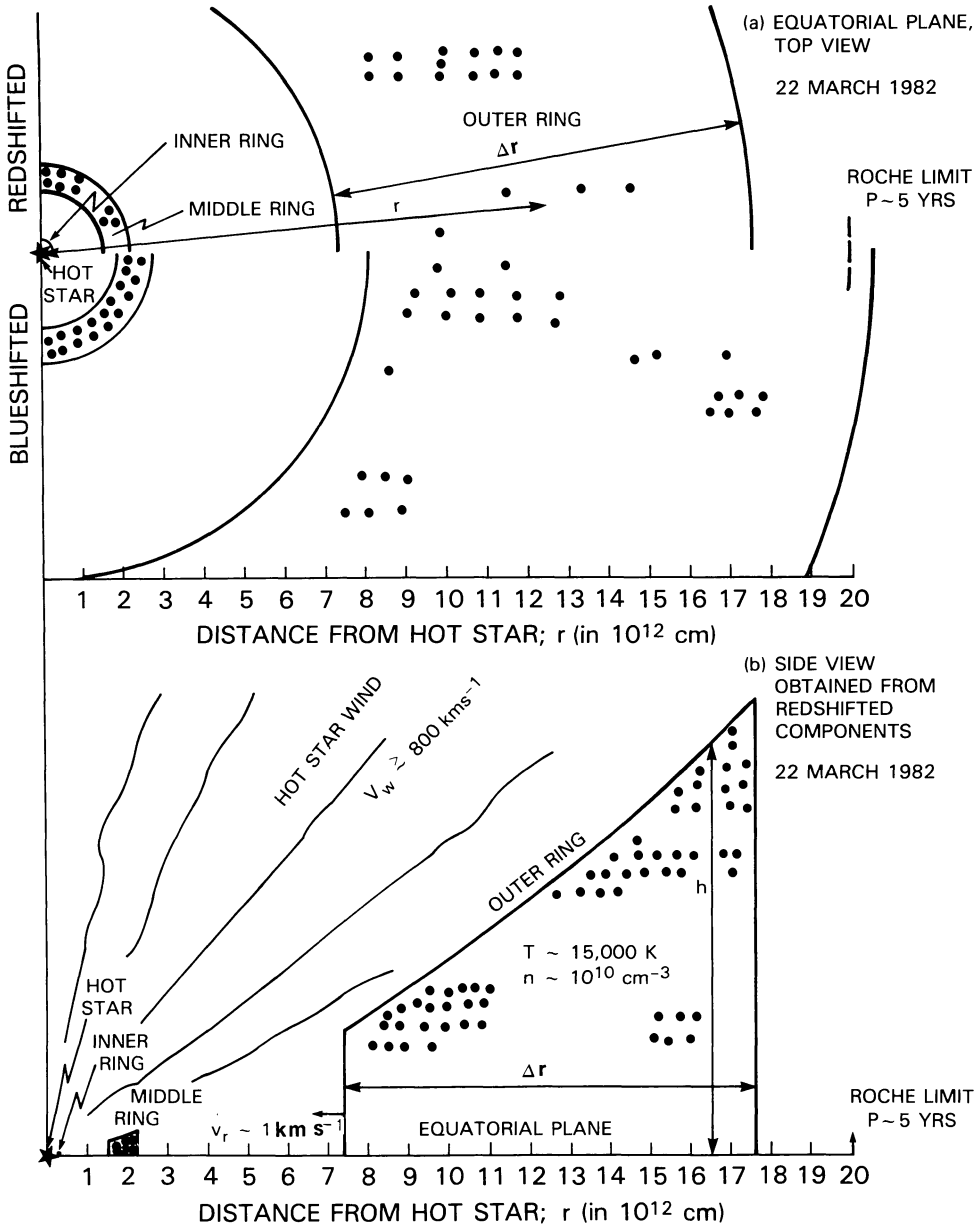

FIG. 4.—Schematic diagram of the ring system deduced from the redshifted and blueshifted components of the C IV profiles for 1982 March 22. The structures of the rings deduced from the blueshifted and redshifted components are not identical, owing to the limiting wavelength uncertainties of the *IUE* SWP spectrometer. (*a*) Top view of equatorial plane: Δr refers to the thickness of the rings; r is the radial distance. (*b*) Side view (obtained from redshifted components). The density and temperature of the outer ring are also shown, as well as the probable radial velocity of infall of the rings. Hot-star wind envelops the entire ring system. The position of the Roche limit of the hot star for a binary period of 5 years is also shown. Note that all rings are inside the Roche limit, as they should be.

redshifted component at $v \sim +35$ km s^{-1} does not have a corresponding blueshifted component. Emission from this feature is probably absorbed by the broad P Cygni profile which arises from the $\gtrsim 800$ km s^{-1} hot-star wind.

Blueshifted components are evident in semiforbidden lines (cf. Si III] structure [Fig. 1*d*, *right-hand panel*]). The component which is generally seen at velocities $\lesssim \pm 10$ km s^{-1} (epochs 1980 September 20, 1982 March 22, 1983 October 29, and 1984 March 11; see Table 3) would be at least $r \gtrsim 1.3 \times 10^{14}$, i.e., outside the Roche limit ($\sim 1.2 \times 10^{13}$ cm) unless the period of the system was exceedingly large, e.g., $P \gtrsim 85$ years. Since it appears either redshifted or blueshifted, it may well be a streamer outside the ring system that is viewed from different angles along the orbital plane. This velocity of $\lesssim 10$ km s^{-1} may also reflect the radial velocity of the system, but the present observations do not enable us to measure it.

In what follows, we adopt a system of at least three rings for which the following scales apply:

$r_1 \sim 10^{13}$ cm, $\Delta r/r \sim 1$ ("outer ring"),

$r_2 \sim 2\times10^{12}$ cm, $\Delta r/r \sim 0.4$ ("middle ring"),

$r_3 \sim 3\times10^{11}$ cm, $\Delta r/r \sim 0.15$ ("inner ring").

The structure follows from the 1982 March 22 data, where the intensities are maximum, and where discrete emission components are most easily seen; similar rings are obtained for the other epochs. Within the observational uncertainties we believe that the rings have remained stationary over a period of ~ 4 years.

The stationary position of the C IV emission components in velocity space enables us to estimate an upper limit to the inflow velocity of the rings, which is ~ 1 km s^{-1}; it could be as small as ~ 0.02 km s^{-1}. It is unlikely that the rings are expanding at either of these velocities because they are much less than the escape velocity from the hot star or the Mira. Since the rings are located inside the Roche limit of the hot secondary, the stationary velocity position of discrete C IV emission components suggests that the radii of the rings are essentially constant, or are slowly contracting.

The origin of the rings is not fully understood at present. However, two possibilities can be considered:

1. Each ring forms during mass-transfer bursts, similar to those proposed for dwarf novae (Bath and Pringle 1981). An accretion disk never fully develops around the secondary. If the stars are in an eccentric orbit, mass transfer could proceed episodically when the stars are at or near periastron. A similar model has been proposed for R Aqr (Kafatos and Michalitsianos 1982). An outburst occurs about every period P, and lasts for a few years. Because RX Pup was in a quiescent state between the 1940s and 1960s, we suspect that the orbital period must be greater than ~ 20 years. From the dimensions of the outer ring deduced from the C IV line-profile data, we conclude that the mass transfer persists for about 11 years.

2. The rings form as a result of instabilities in an accretion disk. For example, if an inner, optically thin radiation-dominated region develops (Novikov and Thorne 1973), the disk can become secularly unstable and break into rings (Lightman and Eardly 1974). These rings form from a disk with thickness greater than the semithickness of the disk. If the radius of the secondary star is about 10^9 cm, the requirement that an optically thin inner region exists implies that the mass accretion rate ($\dot{M}$) is at least 10^{-6} $M_\odot$ yr^{-1}. As we will see below, $\dot{M}$ is generally small, i.e., $\lesssim 10^{-9}$ $M_\odot$ yr^{-1}; but the mass accretion rate can achieve values as large as 10^{-6} $M_\odot$ yr^{-1} during close encounters at periastron, which would result in the disk destabilizing and forming rings. Additionally, thermal instabilities in the disk (Minesize and Osaki 1983) could destabilize the disk and form rings as well. The original disk could have formed during a mass-transfer burst (Bath and Pringle 1981).

We cannot at present distinguish observationally between the two models for ring formation. The mass of the outer ring, however, should be much greater than that of the other inner rings, unless the mass densities of the inner rings are appreciably larger than we estimate (see below). This would indicate that the accretion events that form each ring are not identical with one another.

To get a rough, quantitative estimate of the ring structure, we adopt the second model, which postulates that disk instabilities form rings. By applying the accretion disk formalism, we obtain approximate lower limits for the densities. The drift velocity v_r is given by

$$v_r = \alpha c_s^2 / v_K , \tag{1}$$

where $v_K = (GM_2/r)^{1/2}$ is the Keplerian speed, $M_2 \sim M_\odot$ is the mass of the secondary, and c_s is the sound speed. Using equation (1), we find that the drift time scale,

$$t_r \sim 1.65\times10^7 \alpha^{-1} \times \left[(M_2/M_\odot)(r/10^{13}\ \mathrm{cm})/(T/10^4\ \mathrm{K})\right]^{1/2} \mathrm{s}, \tag{2}$$

should be $t_r \gtrsim 4$ years, and because the temperature in the inner rings is $\gtrsim 15{,}000$ K (see below), we find an upper limit for viscosity $\alpha \sim 1.5\times10^{-2}$. This value of α is appreciably less than the value $\alpha \sim 1$ obtained for dwarf novae or symbiotics, which is based on time-dependent models (Bath and Pringle 1981). Furthermore, a value of $\alpha \sim 1$ would imply that the inner ring would last only ~ 1 year, contrary to these observations.

The mass accretion rate is given by

$$\dot{M} = 4\pi r^2 n m_H \mu \alpha c_s^3 / v_K^2 \tag{3}$$

(cf. Novikov and Thorne 1973), where $\mu \sim 0.65$ is the molecular weight appropriate for an ionized gas. We find that lower limits to the densities in the rings are given by the value

$$n \sim 1.2\times10^{10} (\dot{M}/10^{-9}\ M_\odot\ \mathrm{yr}^{-1})(r/10^{13}\ \mathrm{cm})^{-3} \times (\alpha/1.5\times10^{-2})^{-1}\ \mathrm{cm}^{-3}, \tag{4}$$

and therefore, since the semiforbidden line emission requires that in the outer ring $n \sim 10^{10}$ cm^{-3} (Kafatos, Michalitsianos, and Feibelman 1982), we have $\dot{M} \lesssim 10^{-9}$ $M_\odot$ yr^{-1} for $\alpha \lesssim 1.5\times10^{-2}$.

The rings are expected to be spatially thicker at greater distances from the hot star, since $h/r \sim c_s/v_K$ (Shakura and Sunyaev 1973), i.e.,

$$h/r \sim 0.4\left[(r/10^{13})(T/10^4\ \mathrm{K})/(M_2/M_\odot)\right]^{1/2}. \tag{5}$$

Thus, the outer ring would have a total thickness $2h \sim \Delta r$.

The source of ionization of the rings cannot be an inner accretion disk or a boundary layer. These regions would each

produce a luminosity of

$$\sim 1(\dot{M}/10^{-9}\ M_\odot\ \mathrm{yr}^{-1})(M_2/M_\odot)(R_2/10^9\ \mathrm{cm})^{-1}\ L_\odot, \quad (6)$$

which is not sufficient to photoionize and heat the outer ring. Moreover, the accretion disk theory (Bath *et al.* 1974) predicts very low temperatures in the outer ring. Clearly, temperatures of ~15,000 K in the outer ring (Kafatos, Michalitsianos, and Feibelman 1982) require another source of heating and ionization. We identify this source as the hot star itself. If the mass of the outer ring is $\sim 2.5\times10^{-8}\ M_\odot$, then a photoionizing flux of at least $1.6\times10^{47}\ \mathrm{s}^{-1}$ is required to photoionize it. If $T_2\sim10^5$ K, then $R_2\sim10^{10}$ cm and $L_2\sim2\times10^3\ L_\odot$. The luminosity of the Mira, on the other hand, is $L_1\sim10^4\ L_\odot$. (Kafatos, Michalitsianos, and Feibelman 1982). Such a bright secondary cannot be a main-sequence star, and we identify it instead as a central star of planetary nebula. In the visible, if it were not obscured by the rings and outlying dust, this star would be ~5 mag fainter than the Mira.

We have carried out the analysis of Kafatos, Michalitsianos, and Feibelman (1982) for the UV line emission seen with the *IUE* appropriate for a ring geometry. We find that the largest part of the semiforbidden line intensities comes from the outer ring. We attribute this to the high densities prevalent in the inner two rings ($n\gtrsim10^{12}\ \mathrm{cm}^{-3}$). The inner two rings, however, show emission in allowed lines such as He II λ1640.3 and C IV λλ1548.2, 1550.7. This explains the considerable structure seen in these particular lines. Our analysis yields similar results for the ionic abundances to those obtained by Kafatos, Michalitsianos, and Feibelman (1982). We find that the extinction in the rings is quite high. The values of $E_{B-V}\sim0.3$–0.7 used previously by Kafatos *et al.* may reflect extinction by material either in the outer ring or exterior to it.

The hot-star continuum would dominate the SWP and LWR wavelength ranges if the star were not shrouded by the inner and middle rings. We find that it would be an order of magnitude brighter than the free-free and bound-free continuum discovered by these *IUE* observations and attributed by us to the outer ring. To estimate the magnitude of extinction in the inner two rings, we must know the physical parameters in these rings, i.e., n and T_e. The temperature is probably higher as one moves into the inner rings, but, if the rings are photoionized, T is never near the effective temperature of the hot star, which is ~100,000 K. A more moderate range, from ~10,000 K in the outer regions of the outer ring to $\lesssim$50,000 K in the inner ring, possibly occurs. For this temperature range $n\sim10^{10}\ \mathrm{cm}^{-3}$ (outer ring), $n\sim9\times10^{11}\ \mathrm{cm}^{-3}$ (middle ring), and $n\sim6\times10^{13}\ \mathrm{cm}^{-3}$ (inner ring). Without carrying out radiative transfer calculations, which would be beyond the intended scope of this paper, we estimate that $E_{B-V}\sim1.4$ (inner ring), $E_{B-V}\sim0.35$ (middle ring), and $E_{B-V}\sim0.8$ (outer ring and primarily extinction exterior to the ring system). Had we taken $T\sim15{,}000$ K in all three rings, we would have found $n\sim10^{10}\ \mathrm{cm}^{-3}$, $E_{B-V}\sim1$ (outer ring and primarily extinction exterior to the ring system); $n\sim2\times10^{12}\ \mathrm{cm}^{-3}$, $E_{B-V}\sim0.1$ (middle ring); $n\sim3.7\times10^{14}\ \mathrm{cm}^{-3}$, $E_{B-V}\sim0.7$ (inner ring).

The above estimates of the extinction were obtained by assuming that E_{B-V} is proportional to the column density through the ring $N=\int n\,dr\sim(\Delta r)n$ (cf. Spitzer 1978). Even though the values of density vary greatly in the inner rings, depending upon what temperature structure is assumed, the values of extinction do not. We conclude from the above values of E_{B-V} that the middle, and particularly the inner, rings are intrinsically brighter than the UV emission from the outer ring, particularly in allowed lines. The high values of extinction prevalent in the ring system result in reduced emission in allowed lines (e.g., C IV) from these inner rings. In other words, we find that the C IV intensity should be reduced for higher velocities in the profile, as observed.

We also find that the extinction in the outer ring and outside the system is not sufficient to obscure the stellar continuum radiation, unless we view the rings close to the equatorial plane of the system (within ~8° of the plane), and therefore the velocity structure in the *IUE* high-resolution profiles is the true velocity structure of the rings.

The presence of P Cygni broad absorption in the C IV (as well as He II) lines allows us to determine the properties of the hot-star wind ($v_W\gtrsim800\ \mathrm{km\ s}^{-1}$). We find that $\dot{M}_W\gtrsim2\times10^{-9}\ M_\odot\ \mathrm{yr}^{-1}$ if the wind extends beyond the rings as it should. The mass loss in the wind ($\dot{M}_W$) is suspiciously close to the accretion rate $\dot{M}$ deduced above, and it may well be that the rings, as they fall onto the hot star, power the hot-star wind. The momentum of the hot-star wind is, within a factor of 2 or 3, equal to the momentum of the outer ring (both $\sim6\times10^{29}$ g cm s^{-1}), and it may well be that the hot-star wind pushes out the rings and slows down the accretion. The column density of the wind is $\gtrsim10^{22}\ \mathrm{cm}^{-3}$. We expect that if the momentum of the wind were several times that of the ring, the wind would disrupt the ring system.

In summary, the origin of the ring system suggested in our *IUE* spectra is unknown. We favor episodic mass transfer events from the Mira primary at orbit periastron, since this would result in a periodic phenomenon. The disk never fully develops or, if it does, breaks up into rings by an instability mechanism. The properties of the outer ring are easily obtained, since this ring emits in semiforbidden lines. We find $\Delta r\sim2h\sim r$, $r\sim10^{13}\ \mathrm{cm}^{-3}$, $n\sim10^{10}\ \mathrm{cm}^{-3}$, and $T\sim15{,}000$ K. The middle and inner rings emit primarily in allowed lines, but the high extinction prevalent in them reduces their UV emission and blocks out the hot-star continuum from reaching us, i.e., we view the system close to its orbital plane. The hot star is a luminous central star of a planetary nebula that photoionizes the rings. The rings flow in slowly with $v_r\lesssim1$ km s^{-1}. This slow accretion at rates $\dot{M}\sim10^{-9}\ M_\odot\ \mathrm{yr}^{-1}$ is converted into an outflowing wind that engulfs the entire system. We recommend continuous monitoring of RX Pup in the visible and UV in order to try to determine the orbital period of the system, and to see whether Roche lobe overflow —as we suspect—occurs over time scales of many years. RX Pup offers us a unique opportunity to study the accretion process in D-type symbiotics. The present observations and analysis show that the application of accretion disk theory results in smaller values of viscosity, $\alpha\sim0.01$, than are expected for disks in dwarf novae (Bath and Pringle 1981). The existence of rings is consistant with small values of α, indicative of small viscosity and accretion velocities. Furthermore, low viscosity allows the rings to be persistent features of the RX Pup system over the time scale of these observations.

REFERENCES

Allen, D. A. 1980, *M.N.R.A.S*, **192**, 521.
Barton, J. R., Phillips, B. A., and Allen, D. A. 1979, *M.N.R.A.S.*, **187**, 813.
Bath, G. T., Evans, W. D., Papaloizou, J., and Pringle, J. E., 1974, *M.N.R.A.S.*, **169**, 447.
Bath, G. T., and Pringle, J. E. 1981, *M.N.R.A.S.*, **194**, 967.
Boggess, A., III, *et al.* 1978, *Nature*, **278**, 372.
Feast, M. W., Robertson, B. S. C., and Catchpole, R. M. 1977, *M.N.R.A.S.*, **179**, 499.
Huang, S. S. 1972, *Ap. J.*, **171**, 549.
Kafatos, M., and Michalitsianos, A. G. 1982, *Nature*, **248**, 540.
Kafatos, M., Michalitsianos, A. G., and Feibelman, W. A. 1982, *Ap. J.*, **257**, 204.
Keyes, C. D., and Plavec, M. J. 1980, in *IAU Symposium 88, Close Binary Stars*, ed. M. J. Plavec, D. N. Popper, and R. K. Ulrich (Dordrecht: Reidel), p. 535.
Klutz, M., Simonetto, O., and Swings, J. P. 1978, *Astr. Ap.*, **66**, 283.
Klutz, M., and Swings, J. P. 1981, *Astr. Ap.*, **96**, 406.
Kwok, S. 1982, in *IAU Colloquium 70, The Nature of Symbiotic Stars*, ed. M. Friedjung and R. Viotti (Dordrecht: Reidel), p. 17.
Lightman, A. P. and Eardly, D. M. 1974, *Ap. J. (Letters)*, **187**, L1.
Minesize, S., and Osaki, Y. 1983, *Pub. A.S.P.*, **35**, 337.
Mueller, B. E. A., and Nussbaumer, H. 1985, *Astr. Ap.*, **143**, 144.
Novikov, J. D., and Thorne, K. S. 1973, in *Black Holes*, ed. C. DeWitt and B. S. DeWitt (New York: Gordon & Breach), p. 343.
Penston, M. V., and Allen, D. A. 1985, *M.N.R.A.S.*, **212**, 939.
Shakura, N. I., and Sunyaev, R. A. 1973, *Astr. Ap.*, **24**, 337.
Smak, J. 1969, *Acta Astr.*, **19**, 155.
Spitzer, L., Jr. 1978, *Physical Processes in the Interstellar Medium* (New York: Wiley), p. 3.
Swings, J. P., and Struve, O. 1941, *Ap. J.*, **94**, 291.
Wallerstein, G. 1978, *Pub. A.S.P.*, **90**, 36.
Wallerstein, G., Willson, L. A., Salzer, J., and Brugel, E. 1984, *Astr. Ap.*, **133**, 137.
Whitelock, P. A., Catchpole, R. M., Feast, M. W., Roberts, G., and Carter, B. S. 1983, *M.N.R.A.S.*, **203**, 363.
Willson, L. A., Wallerstein, G., Brugel, E. W., and Stencel, R. E. 1984, *Astr. Ap.*, **133**, 154.

R. P. FAHEY and A. G. MICHALITSIANOS: Laboratory for Astronomy and Solar Physics, Code 684 NASA/Goddard Space Flight Center, Greenbelt, MD 20771

M. KAFATOS: Department of Physics, George Mason University, Fairfax, VA 22030